High-Resolution Integrated Microfluidic Probe for Mass Spectrometry Imaging of Biological Tissues

Xiangtang Li, Hang Hu, Julia Laskin*

Department of Chemistry, Purdue University, West Lafayette, IN 47907, United States

ABSTRACT: Nanospray desorption electrospray ionization (nano-DESI) is an ambient ionization technique that enables molecular imaging of biological samples with high spatial resolution. We have recently developed an integrated microfluidic probe (iMFP) for nano-DESI mass spectrometry imaging (MSI) that significantly enhances the robustness of the technique. Herein, we report the design and performance of a second-generation iMFP for imaging with high spatial resolution. The new iMFP features smaller primary and spray channels and a new configuration of the sampling port that enables robust imaging of tissues with a spatial resolution of 8-10 μm. We demonstrate the spatial resolution, sensitivity, durability, and throughput of the iMFP by imaging mouse uterine and brain tissue sections. With a scan rate of 0.2 mm/s, we obtained high-resolution images of a mouse uterine tissue section (scanned area: 2.9 mm × 3.2 mm) in less than 29 minutes without sacrificing sensitivity. This corresponds to a 10-fold improvement in the experimental throughput in comparison with previously reported high-resolution nano-DESI MSI experiments. Overall, the new probe design opens opportunities for mapping biomolecules in biological samples with high throughput and cellular resolution, which is important for understanding biological systems.

Mass spectrometry imaging (MSI) is a powerful analytical tool for applications in life sciences. MSI enables label-free spatial mapping of molecules thereby providing detailed molecular maps of biological systems.[1-5] Despite the power of MSI, imaging with high spatial resolution is still challenging. Secondary ion mass spectrometry (SIMS) offers the best spatial resolution of ~2 μm for imaging of biomolecules in tissues.[6, 7] Meanwhile, tissue imaging using matrix-assisted laser desorption ionization (MALDI), the most commonly used ionization technique in MSI, is typically performed with a spatial resolution, ranging from 20 μm to 50 μm. Several studies have demonstrated MALDI imaging with a spatial resolution of better than 10 μm[8-12] with the smallest pixel size of 1.4 μm achieved using a specially-designed atmospheric pressure MALDI source.[11] Meanwhile MALDI MSI in a transmission geometry has been used for imaging of proteins with a spatial resolution of 2.5 μm.[10] More recently, transmission mode MALDI, in which the ionization of desorbed analytes is enhanced by a second laser referred to as "MALDI-2" has been used to attain a pixel size of 600 nm.[13]

Ambient ionization techniques[14-16] enable imaging of biological samples without special sample pre-treatment but often are limited in the achievable spatial resolution. For example, desorption electrospray ionization (DESI)[17] imaging is typically performed with a spatial resolution of 100-200 μm with a best value of 35 μm achieved by carefully optimizing the experimental parameters.[18] Recent developments of a DESI probe with electro-flow focusing have substantially improved the sensitivity, spatial resolution, and robustness of this ambient imaging technique.[19] Infrared matrix assisted electrospray ionization (IR-MALDESI) has been used for tissue imaging with 55 μm resolution.[20] Meanwhile, liquid extraction surface analysis (LESA),[21] and liquid microjunction surface sampling probe (LMJ-SSP),[22] have been used for imaging with a spatial resolution of 1 mm and 0.5 mm, respectively. Recent developments of ambient ionization imaging platforms based on nanospray desorption electrospray ionization (nano-DESI),[23-26] single probe,[27] fiber probe laser ablation dielectric barrier discharge,[28] and tapping-mode scanning probe electrospray ionization[29] have enabled imaging of biological samples with a spatial resolution of better than 10 μm.

Nano-DESI, is a liquid extraction-based ambient ionization approach, [23] which has been used for imaging of biological tissues with a spatial resolution of better than 10 μm.[25, 26] In a conventional nano-DESI experiment, analytes are extracted into a dynamic liquid bridge formed between two fused silica capillaries and ionized at a mass spectrometer inlet using electrospray or nanoelectrospray ionization. Imaging with high spatial resolution is performed by finely pulling the capillaries and incorporating a shear force probe that controls the distance to the sample to within 1 μm.[25, 30, 31] Nano-DESI MSI has been extensively used for imaging of lipids, drugs, and metabolites.[32-38] Furthermore, concentration gradients of alkali metal cations have been measured by adding a complexation agent to the extraction

solvent.[39] Recent advances have focused on imaging of proteoforms in biological tissues with both moderate [40-43] and high spatial resolution[44] thereby considerably expanding the range of applications of this technique.

We have developed an integrated microfluidic probe (iMFP) for nano-DESI MSI experiments, which simplifies the alignment of the probe in front of a mass spectrometer while providing a comparable performance to the capillary-based probe.[45] The iMFP is microfabricated using glass and contains a primary and spray channels that form a sampling port positioned on a sample surface. The first generation iMFP has been used for imaging of tissue sections with a spatial resolution of ~25 μm.[45] In addition, we have developed an iMFP for high-throughput MSI experiments.[46] This probe features larger channels and a geometry of the sampling port optimized for stable performance of the iMFP at high scan rates.[46] Using this probe, we achieved a 5-10 fold increase in the experimental throughput, which can be further increased using the dynamic sparse sampling approach reported in our recent studies.[47, 48]

In this study, we describe the design of a high-resolution iMFP for nano-DESI MSI experiments. This probe features smaller channels and a specially designed configuration of the sampling port that a small and stable liquid bridge on the sample surface. By optimizing the iMFP design, we achieved a spatial resolution of 8-10 μm and a 10-fold increase in the experimental throughout in comparison with previous high-resolution nano-DESI MSI experiments.

EXPERIMENTAL SECTION

Chemicals and Solvent Preparation

LC-MS grade methanol (MeOH) and Omnisolv LC-MS grade water were purchased from MilliporeSigma (Burlington, MA). Lysophosphatidylcholine 19:0 (LPC 19:0) was purchased from Avanti Polar Lipids (Alabaster, AL). The extraction solvent in this study was composed of a 9:1 MeOH-water mixture containing 1 μM LPC 19:0 as an internal standard.

Biological Tissues

Biological tissue sections were available from our previous studies.[10, 17, 22, 38] We used mouse uterine tissue on day 4 of pregnancy sliced to a series of sections with a thickness of 12 μm, thaw-mounted onto pre-cleaned polylysine coated microscope glass slides, and stored at –80 °C. Rat brain tissue sections from Wistar Han rat that were provided by Merck & Co. and stored at –80 °C freezer until the analysis.

Fabrication of the high resolution iMFP

The microfluidic chip is manufactured as described in our previous studies[45, 46] using traditional photolithography, wet etching, and high-temperature bonding.[49] **Figure S1** shows a photomask used to fabricate the channel pattern on a glass substrate; the fabrication procedure described in prior publications[45, 46] is illustrated in **Figure S2**. Briefly, a chromium (Cr) layer is deposited onto a glass substrate and positive photoresist is spin-coated onto the Cr surface. A photomask is placed on top of the photoresist layer and the channel pattern is generated by exposing the surface to the UV light. The photoresist and Cr layers in the areas exposed to the UV light are removed by treating the substrate wih AZ developer and etching with Cr etchant. Next, the microchannels patterned onto the glass substrate are etched to generate the channels and the unexposed photoresist and Cr layer are removed. A blank cover plate is placed on top of the substrate plate with the channels and the two plates are bonded at 590 ℃ for ~3 hours. The final channel dimensions are shown in **Figure 1**. The 40 μm-wide, 15 μm-deep solvent channel (40 ×15 μm) is terminated with a 1.5 mm-long 30 × 15 μm section. The spray channel has the same dimensions of ~30 × 15 μm throughout its length. The port through which an external fused silica capillary (inner diameter (ID) of 50 μm and outer diameter (OD) of 150 μm, Molex, Thief River Falls, MN) is connected to the iMFP is polished with an 150 μm in diameter electric drill head to a depth that can accommodate the capillary.

The sampling port and nanospray emitter of iMFP are then created through a multistep grinding and polishing of the microfluidic chip using a power tool and sandpaper. A fused silica capillary (50 μm ID, 150 μm OD) that propels the extraction solvent from the syringe pump is attached to the iMFP using an epoxy glue. The epoxy is coated uniformly on the outer surface of the fused silica capillary about two millimeters above its end and is allowed to dry. When the epoxy becomes semi-dry, the capillary is inserted into the solvent channel of the probe and pushed to the end of the channel to eliminate dead volume. The epoxy is allowed to dry for 24 hrs. Prior to the initial usage of the iMFP, the solvent channel, spray channel and sampling port are treated for 5 min with a 5:1:1 (v/v/v) H_2O/HCl/H_2O_2 solution. Before each imaging experiment, the channels and sampling port of the probe are vacuum-suctioned for five minutes while being flushed with deionized water, 0.1 M HCl, 0.1 M NaOH, and deionized water once more. This process is repeated three times.

The iMFP-Based Nano-DESI Imaging Platform

The nano-DESI MSI platform is comprised of a syringe pump with a 2.5 mL syringe for solvent delivery, a micropositioner for the iMFP, a sample holder, an XYZ motorized stage (Zaber, Technologies, Vancouver, BC) for positioning the sample holder, and one Dino-Lite digital microscope for monitoring the iMFP during imaging experiments.[25] The microscope is focused on the sampling port and monitors the nanospray emitter tip and MS inlet. The iMFP is mounted onto a micropositioner and positioned in front of a mass spectrometer inlet. The distance between the nanospray emitter tip and the MS inlet orifice is ~0.5 mm.

The fused silica capillary attached to the iMFP is connected to a syringe pump. The syringe pump propels the solvent at a flow rate of 1.0 µL/min. The spray voltage of +3.2 kV is applied to the syringe needle using a high-voltage cable. A 10-MΩ resistor is integrated into the high-voltage cable to avoid potential electric shock. For safety reasons, the users must switch the instrument to the standby mode before touching the crocodile clip of the high voltage cable.

A microscope glass slide containing tissue sections is placed onto the sample holder. A custom LabVIEW software controls the movement of the XYZ stage, which is used for sample positioning. The extraction solvent is driven via the iMFP to the sampling port, which is positioned to form a small and stable liquid bridge on the sample surface; the extracted analyte molecules are then transferred by the solvent to a mass spectrometer through the spray channel.

Mass Spectrometry Imaging Experiments

Nano-DESI MSI experiments were performed in positive ionization mode using a Q-Exactive HF-X mass spectrometer (Thermo Scientific, Bremen, Germany). The parameters of the ionization source were as follows: high voltage, +3.2 kV; RF funnel voltage, +100 V; temperature of the heated capillary, 300 °C. Mass spectra were acquired in the range of *m/z* of 133−2000 with a mass resolution of 60,000 at *m/z* 200. The AGC target was 1×10^6 and the maximum injection time was 200 ms. MSI data were acquired in lines by scanning the sample under the iMFP using the XYZ stage and stepping between the lines. The distance between the iMFP and sample was controlled using the "three-point plane" method.[50] This method automatically compensates for the tilt of the sample surface using the coordinates of three points outside of the tissue section. The coordinates of the three points are defined by landing the iMFP on the glass surface. High resolution imaging experiments of mouse uterine tissue sections were performed using a scan rate of 0.02 mm/s and the step between the lines of 15 µm. Imaging of rat brain tissue sections was performed using a scan rate of 0.02 mm/s and 20 µm spacing between the lines. High throughput imaging of a mouse uterine tissue section was performed using a scan rate of 0.2 mm/s with a 20 µm spacing between the lines.

Data Analysis

Each line scan was acquired as an individual RAW data file using Xcalibur software. A custom-designed Python code (https://github.com/LabLaskin/MSI-image-generator) was used to visualize ion images. RAW data files were processed using pyMSfilereader. Ion signals of each selected *m/z* feature were extracted from mass spectra using a mass tolerance window of ±10 ppm, normalized to the total ion current (TIC), and aligned with respect to sampling locations. The alignment is necessary because of the differences in the acquisition time of individual mass spectra corresponding to individual pixels in the image. The identification of phospholipids and metabolites observed in imaging experiments was performed based on the accurate mass measurement and MS/MS data obtained directly on a tissue section.

RESULTS AND DISCUSSION

The size and stability of the liquid bridge on a sample surface determines the spatial resolution of nano-DESI MSI experiments. Meanwhile, the stability of the ion signal affects the experimental sensitivity and quality of the imaging data. The design of the high-resolution iMFP is illustrated in **Figures 1A-D**. We have redesigned the sampling port of the iMFP to ensure that the volume of the liquid bridge is small and remains constant throughout the imaging experiment. Specifically, we have fabricated the iMFP, in which part of the solvent channel has the dimensions of 40 µm × 15 µm and another part at the sampling port has the same dimensions of 30 µm × 15 µm as the spray channel. We note that both channels are smaller

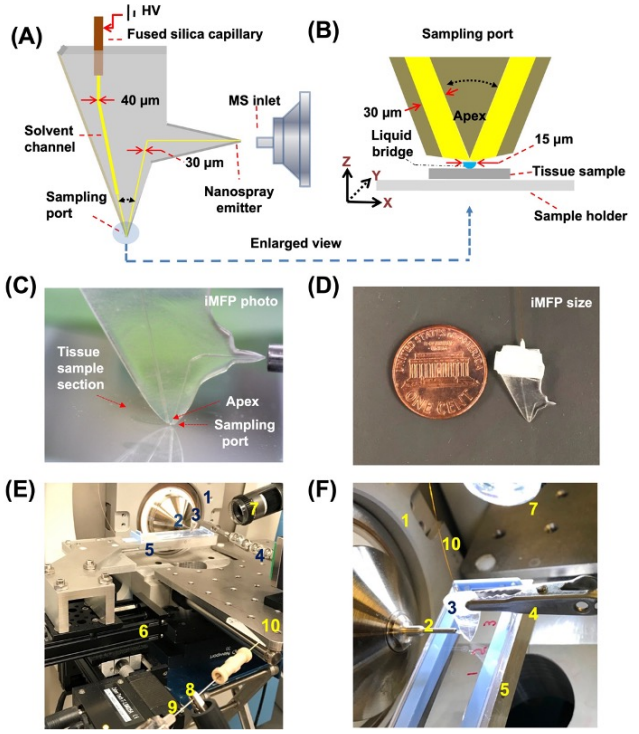

Figure 1. (A) A schematic drawing of the high-resolution iMFP; (B) A schematic illustration of the sampling port and liquid bridge between the probe and sample surface; (C) A photograph of the iMFP in front of a mass spectrometer inlet and the sampling port on top of a glass surface near the tissue sample; (D) A photograph showing the size of the iMFP; (E) and (F) Photographs of the iMFP-based imaging platform in front of a mass spectrometer showing: 1, instrument mounting flange; 2, extended ion transfer tube; 3; the iMFP; 4, XYZ inline micro-positioner; 5, sample holder; 6, motorized XYZ stage; 7, Dino-Lite microscope; 8, high-voltage connector; 9, syringe delivering the working solvent; 10, fused-silica capillary (50 µm i.d) supplying the working solvent to the iMFP.

than the 40 µm × 25 µm channels used in the previous design.[45] Furthermore, we reduced the length of the spray channel to 7 mm, which shortens the transfer time to the instrument inlet thereby preventing signal tailing (**Figure 1D**). This design, in which the width of the solvent channel decreases from 40 µm near the external capillary to 30 µm at the sampling port makes it easier to connect the external capillary to the small probe. The design of the sampling port (**Figure 1B**) is one of the novel aspects of the high-resolution iMFP. In this design, the apex of the sampling port is at the same height as the opening of the iMFP, which brings the apex in direct contact with the sample surface when the probe lands onto it **(Figure 1B, 1C)**. This geometry helps minimize the size of the liquid bridge while maintaining its stability.

Extraction of molecules into the liquid bridge is followed by their soft, electrospray-like ionization. The stability of the Taylor cone is determined by the geometry of the monolithic nanospray emitter produced by grinding and polishing. The alignment of the probe in front of the mass spectrometer inlet and the components of the imaging platform are shown in **Figures 1E** and **1F**, respectively.

In addition to the probe design, we have optimized several parameters including high voltage, flow rate, and distance between the iMFP and sample surface that affect the performance of high-resolution MSI experiments.[46] The stability of the liquid bridge is critical to nano-DESI imaging with high spatial resolution. The flow rate of the solvent and distance between the nano-DESI probe and sample surface must be carefully optimized and precisely controlled throughout the experiment. Two different strategies for the constant distance mode nano-DESI MSI have been reported in our previous studies.[30, 50] The most straightforward method uses a three-point plane approach to compensate for the tilt of the sample surface during the experiment.[50] This method works particularly well for samples that are flat. Another method relies on a shear force feedback to control the distance between the sample and nano-DESI probe.[30, 31] This allows for high-resolution imaging of tissues as well as imaging of materials with complex topography.[31]

In this work, high resolution MSI experiments were performed using the "three-point plane" approach. The acquisition parameters used for imaging of different tissues are summarized in **Table S1**. Most of the experiments were performed using a high voltage of 3.2 kV, flow rate of 1.1 µL/min, and scan rate of 0.02 mm/s. At higher scan rates, the flow rate was increased to ensure the stability of the liquid bridge. For example, flow rates of 1.1 and 1.3 µL/min were used for imaging at scan rates of 0.02 and 0.2 mm/s, respectively.

We demonstrate the performance of the high-resolution iMFP using mouse uterine tissue as a model system.[25] This tissue contains different cell types that generate distinct chemical gradients in a small area of ~2 mm in diameter. Ion

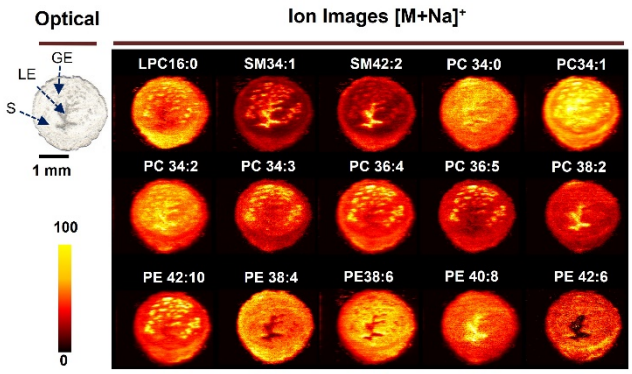

Figure 2. Optical image of a mouse uterine tissue section and representative positive mode ion images of phospholipids acquired using the high-resolution iMFP. PC, LPC, SM, and PE represent phosphatidylcholine, lysophosphatidylcholine, sphingomyelin, and phosphatidylethanolamine, respectively. Scale bar is 1 mm. The intensity scale changes from black (low) to yellow (high). Abbreviation: luminal epithelium (LE), glandular epithelial cells (GE), stroma that surrounds LE and GE (S).

images obtained for this tissue type using the high-resolution iMFP are shown in **Figure 2**. The results are comparable to previous reports[25, 45] showing distinct patterns of phospholipid localization to the stroma, luminal epithelium (LE), and glandular epithelial cells (GE). For example, signals of several species including PC 38:2, SM 42:2, and PE 40:8 are enhanced in the LE region. Meanwhile, signals of LPC 16:0, SM 34:1, PC34:3, PC 36:4, PC 36:5, and PE 42:10 are enhanced in the GE and LE regions. Other species including PE 38:4, PE 38:6, and PE 42:6 show low signals in the LE region and are evenly distributed in the other parts of the tissue.

We estimate the spatial resolution using the "20-80" rule, in which the resolution is defined as the distance over which the signal of a selected ion changes between 20% and 80% of its maximum value.[51, 52] We use the sharpest chemical gradients observed in the experimental data to estimate the upper limit of the spatial resolution. In this study, we used an ion image of SM 34:1 (**Figure 3A**), which shows a

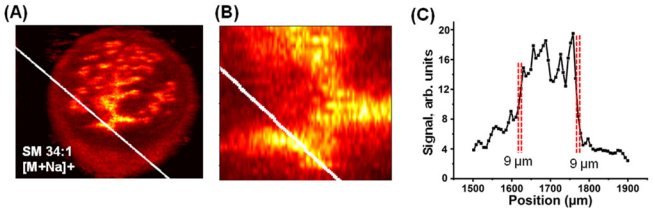

Figure 3. Estimation of the spatial resolution using an ion image of the $[M+Na]^+$ ion of SM 34:1 normalized to the TIC (A). Line profile was extracted along the white line. (B) An expanded view of the region between LE and stroma regions. (C) An example of a line profile used to estimate the spatial resolution based on the steepest chemical gradients. Red dashed lines highlight the regions over which the signal changes between 20% and 80% of its maximum span.

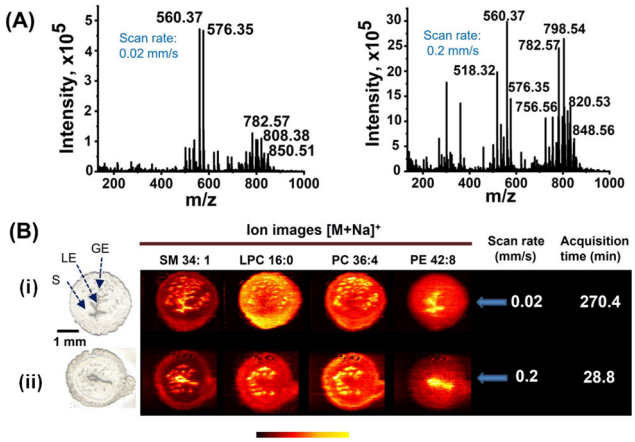

Figure 4. (A) Single-pixel mass spectra obtained using the high-resolution iMFP at two scan rates of 0.02 and 0.2 mm/s showing comparable sensitivity. (B) Representative positive ion images obtained for mouse uterine tissue sections at scan rates of (i) 0.02 and (ii) 0.2 mm/s. Scale bar is 1 mm; The intensity scale changes from black (low) to yellow (high).

distinct localization in the mouse uterine tissue to estimate the spatial resolution of the iMFP. By examining line scans through the transition regions between LE and stroma (**Figure 3B**), we estimate the spatial resolution in the range of 8-10 µm as shown in **Figure 3C**. Based on these results, we conservatively estimate that the upper limit of the spatial resolution obtained in this study is ~10 µm.

The robustness of the high-resolution iMFP allowed us to achieve a comparable quality performance at the scan rates of 0.02 and 0.2 mm/s as shown in **Figure 4**. Single-pixel mass spectra shown in **Figure 4A** indicate that the signals of the extracted analytes do not decrease at a higher scan rate. Meanwhile, ion images shown in **Figure 4B** confirm that both the spatial resolution and quality of imaging data remain the same at 0.02 and 0.2 mm/s scan rates. This

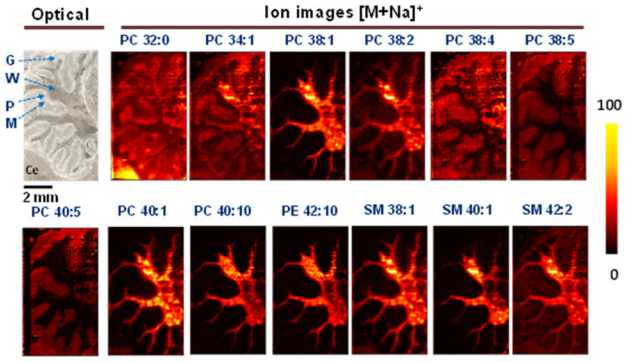

Figure 5. An optical image of the cerebellum region of a mouse brain tissue section analyzed in this study and representative positive mode ion images of endogenous molecules in the tissue. Each image corresponds to a sodium adduct $[M+Na]^+$ of a unique phospholipid. Blue arrows highlight the molecular layer (M), Purkinje layer (P), granular layer (G), and white matter (W). Scale bar is 2 mm; The intensity scale changes from black (low) to yellow (high).

observation is consistent with the results reported in our previous study.[46] It follows that, using the high-resolution iMFP, we achieved a 10-fold improvement in the experimental throughput without loss of sensitivity and spatial resolution. This is the first demonstration of nano-DESI imaging with both high spatial resolution and throughput, which is enabled by the robustness of the probe design that provides stable signals even at high scan rates.

To explore the robustness of the high-resolution iMFP and its utility for high-resolution imaging of larger tissue sections, we examined a 4 mm × 6 mm region of a mouse brain tissue in the cerebellum region. This experiment was performed at a scan rate of 20 µm/s and a step between the lines of 20 µm corresponding to the total acquisition time of 980 min (16.3 hrs). A stable signal was obtained throughout the experiment highlighting the robustness of the probe. An optical image of the section and representative positive mode ion images are shown in **Figure 5**. Four regions of the cerebellum including the white matter, granular layer, Purkinje layer, and molecular layer are marked with blue arrows in the optical image of the tissue section in **Figure 5**.

Ion images of endogenous molecules in the cerebellum region shown in **Figure 5** indicate that most of the phospholipids show an enhanced abundance in the white matter region. Among the phospholipids enhanced in the grey matter, PC 32:0 is present in lower abundance in the molecular layer and is uniformly distributed in both the granular and Purkinje layers. Meanwhile, PC 38:5 and PC 40:5 are observed in the molecular layer and show low signals in all other regions of the cerebellum. Another distinct localization pattern is displayed by PC 34:1, which is observed in the grey matter and shows an enhanced signal in the white matter region. These results are in general agreement with previously published data.[13, 53, 54]

Several phospholipids including PC 38:1, PC 38:2, PC 40:1, PC 40:10, SM 38:1, SM 40:1, and PE 42:10 show a distinct localization in the white matter region. Some of these species including PC 38:1 and PC 40:1 are known to be associated with oligodendrocytes[55] — lipid-rich cells in the central nervous system that produce myelin sheath.[56] Specifically, lipidomics experiments have demonstrated that concentrations of several phosphatidylcholines including PC38:1, PC38:4, PC40:1, PC42:1, and PC42:2 are substantially lower in mice with conditional deletion of meningioma-expressed antigen 6 (Mea6) in oligodendrocytes, which impairs the development of the white matter.[55] These observations indicate an important yet still poorly understood role of PC species in myelination.[56] The newly-developed high-resolution iMFP opens an opportunity to explore the role of phospholipids in the central nervous system by examining their spatial localization to specific cell types.

CONCLUSIONS

We have developed a high-resolution microfluidic probe, iMFP, for nano-DESI MSI. To achieve a high spatial resolution, we reduced the dimensions of the channels in the probe and designed the sampling port, which generates a small and stable liquid bridge on the sample surface. This is achieved by bringing the apex of the probe close to the opening of the sampling port. Using this new probe design, we achieved a spatial resolution of 8-10 μm. Furthermore, we demonstrated that the high-resolution probe may be used for imaging with higher throughput without any loss in sensitivity. The robustness of the probe was examined by imaging a large mouse brain tissue section with high spatial resolution over the course of 16 hrs. This experiment provided insights into the regional distribution of cells within specific molecular layers of the cerebellum region of a mouse brain tissue using phospholipids that display distinct localization to oligodendrocytes in the white matter region. Further improvement in spatial resolution of the iMFP may be achieved by (1) reducing the dimensions and shortening the length of the spray channel; (2) regulating the distance between the sampling port and sample surface using the shear force probe feedback, and (3) developing an even smaller sampling port by changing the angle between the channels or reducing the size of the probe. In summary, the iMFP enables imaging of lipids and metabolites in biological tissues with high sensitivity, spatial resolution, and throughput. The new probe design will enable mapping of biomolecules in biological samples with a subcellular resolution, which is important for obtaining a detailed understanding of biochemical processes of interest to molecular biology, drug discovery, and clinical research.

SUPPORTING INFORMATION

Supporting information providing additional details related to device fabrication and experimental parameters, is available free of charge on the ACS Publications website.

AUTHOR INFORMATION

Corresponding Author

* Prof. Julia Laskin
Department of Chemistry, Purdue University
560 Oval Drive, West Lafayette, IN 47907 (USA)
E-mail: jlaskin@purdue.edu
TEL: 765-494-5464.

Notes

The authors have no conflict of interest to declare.

ACKNOWLEDGMENTS

The authors gratefully acknowledge the financial support from the National Institutes of Health (NIH) Common Fund, through the Office of Strategic Coordination/Office of the NIH Director under award UG3HL145593 and UH3CA255132 (HuBMAP Program) and RF1MH128866 (BICCN Program). HH acknowledges the support from the HuBMAP's jump-start award. We would like to thank Joon Hyeong Park (the Birck Nanotechnology Center, Purdue University) for helpful discussions and technical assistance with the development of the photomask. We are also grateful to Dr. Yingju Li, Prof. Xiaofei Sun, Prof. Sudhansu K. Dey from Cincinnati Children's Hospital Medical Centre for providing mouse uterine tissue samples and Dr. Bingming Chen from Merck for providing rat brain tissue sections.

REFERENCES

(1) Stoeckli, M.; Chaurand, P.; Hallahan, D. E.; Caprioli, R. M. Imaging mass spectrometry: a new technology for the analysis of protein expression in mammalian tissues. *Nature medicine* **2001**, *7*, 493-496.
(2) McDonnell, L. A.; Heeren, R. M. Imaging mass spectrometry. *Mass Spectrom. Rev.* **2007**, *26*, 606-643.
(3) Wu, C.; Dill, A. L.; Eberlin, L. S.; Cooks, R. G.; Ifa, D. R. Mass spectrometry imaging under ambient conditions. *Mass Spectrom. Rev.* **2013**, *32*, 218-243.
(4) Norris, J. L.; Caprioli, R. M. Analysis of tissue specimens by matrix-assisted laser desorption/ionization imaging mass spectrometry in biological and clinical research. *Chem. Rev.* **2013**, *113*, 2309-2342.
(5) Buchberger, A. R.; DeLaney, K.; Johnson, J.; Li, L. Mass spectrometry imaging: a review of emerging advancements and future insights. *Anal. Chem.* **2018**, *90*, 240.
(6) Winograd, N. Gas Cluster Ion Beams for Secondary Ion Mass Spectrometry. In *Annual Review of Analytical Chemistry, Vol 11*, Bohn, P. W., Pemberton, J. E. Eds.; Annual Review of Analytical Chemistry, Vol. 11; 2018; pp 29-48.
(7) Boxer, S. G.; Kraft, M. L.; Weber, P. K. Advances in imaging secondary ion mass spectrometry for biological samples. *Annual review of biophysics* **2009**, *38*, 53-74.
(8) Zavalin, A.; Todd, E. M.; Rawhouser, P. D.; Yang, J.; Norris, J. L.; Caprioli, R. M. Direct imaging of single cells and tissue at sub-cellular spatial resolution using transmission geometry MALDI MS. *J. Mass Spectrom.* **2012**, *47*, 1473-1481.
(9) Rompp, A.; Spengler, B. Mass spectrometry imaging with high resolution in mass and space. *Histochemistry and Cell Biology* **2013**, *139*, 759-783. DOI: 10.1007/s00418-013-1097-6.
(10) Zavalin, A.; Yang, J.; Hayden, K.; Vestal, M.; Caprioli, R. M. Tissue protein imaging at 1 μm laser spot diameter for high spatial resolution and high imaging speed using transmission geometry MALDI TOF MS. *Analytical and bioanalytical chemistry* **2015**, *407*, 2337-2342.
(11) Kompauer, M.; Heiles, S.; Spengler, B. Atmospheric pressure MALDI mass spectrometry imaging of tissues and cells at 1.4-μm lateral resolution. *Nat. Methods* **2017**, *14*, 90-96.

(12) Spivey, E. C.; McMillen, J. C.; Ryan, D. J.; Spraggins, J. M.; Caprioli, R. M. Combining MALDI-2 and transmission geometry laser optics to achieve high sensitivity for ultra-high spatial resolution surface analysis. *J. Mass Spectrom.* **2019**, *54*, 366-370.
(13) Niehaus, M.; Soltwisch, J.; Belov, M.; Dreisewerd, K. Transmission-mode MALDI-2 mass spectrometry imaging of cells and tissues at subcellular resolution. *Nat. Methods* **2019**, *16*, 925-931.
(14) Li, N.; Nie, H.; Jiang, L.; Ruan, G.; Du, F.; Liu, H. Recent advances of ambient ionization mass spectrometry imaging in clinical research. *J. Sep. Sci.* **2020**, *43*, 3146-3163.
(15) Venter, A. R.; Douglass, K. A.; Shelley, J. T.; Hasman Jr, G.; Honarvar, E. Mechanisms of real-time, proximal sample processing during ambient ionization mass spectrometry. *Anal. Chem.* **2014**, *86*, 233-249.
(16) Laskin, J.; Lanekoff, I. Ambient mass spectrometry imaging using direct liquid extraction techniques. *Anal. Chem.* **2016**, *88*, 52-73.
(17) Takats, Z.; Wiseman, J. M.; Gologan, B.; Cooks, R. G. Mass spectrometry sampling under ambient conditions with desorption electrospray ionization. *Science* **2004**, *306*, 471-473.
(18) Campbell, D. I.; Ferreira, C. R.; Eberlin, L. S.; Cooks, R. G. Improved spatial resolution in the imaging of biological tissue using desorption electrospray ionization. *Analytical and bioanalytical chemistry* **2012**, *404*, 389-398.
(19) Wu, V.; Tillner, J.; Jones, E.; McKenzie, J. S.; Gurung, D.; Mroz, A.; Poynter, L.; Simon, D.; Grau, C.; Altafaj, X. High Resolution Ambient MS Imaging of Biological Samples by Desorption Electro-Flow Focussing Ionization. *Anal. Chem.* **2022**, *94*, 10035-10044.
(20) Joignant, A. N.; Bai, H.; Manni Sr, J. G.; Muddiman, D. C. Improved Spatial Resolution of Infrared Matrix-Assisted Laser Desorption Electrospray Ionization (IR-MALDESI) Mass Spectrometry Imaging (MSI) Using a Reflective Objective. *Rapid Commun. Mass Spectrom.* **2022**, e9392.
(21) Swales, J. G.; Tucker, J. W.; Spreadborough, M. J.; Iverson, S. L.; Clench, M. R.; Webborn, P. J.; Goodwin, R. J. Mapping drug distribution in brain tissue using liquid extraction surface analysis mass spectrometry imaging. *Anal. Chem.* **2015**, *87*, 10146-10152.
(22) Van Berkel, G. J.; Kertesz, V.; Koeplinger, K. A.; Vavrek, M.; Kong, A. N. T. Liquid microjunction surface sampling probe electrospray mass spectrometry for detection of drugs and metabolites in thin tissue sections. *J. Mass Spectrom.* **2008**, *43*, 500-508.
(23) Roach, P. J.; Laskin, J.; Laskin, A. Nanospray desorption electrospray ionization: an ambient method for liquid-extraction surface sampling in mass spectrometry. *Analyst* **2010**, *135*, 2233-2236.
(24) Laskin, J.; Heath, B. S.; Roach, P. J.; Cazares, L.; Semmes, O. J. Tissue imaging using nanospray desorption electrospray ionization mass spectrometry. *Anal. Chem.* **2012**, *84*, 141-148.
(25) Yin, R.; Burnum-Johnson, K. E.; Sun, X.; Dey, S. K.; Laskin, J. High spatial resolution imaging of biological tissues using nanospray desorption electrospray ionization mass spectrometry. *Nature Protocols* **2019**, *14*, 3445-3470.
(26) Yin, R. C.; Kyle, J.; Burnum-Johnson, K.; Bloodsworth, K. J.; Sussel, L.; Ansong, C.; Laskin, J. High Spatial Resolution Imaging of Mouse Pancreatic Islets Using Nanospray Desorption Electrospray Ionization Mass Spectrometry. *Anal. Chem.* **2018**, *90*, 6548-6555. DOI: 10.1021/acs.analchem.8b00161.
(27) Pan, N.; Rao, W.; Kothapalli, N. R.; Liu, R.; Burgett, A. W.; Yang, Z. The single-probe: a miniaturized multifunctional device for single cell mass spectrometry analysis. *Anal. Chem.* **2014**, *86*, 9376-9380.
(28) Lu, Q.; Guan, X.; You, X.; Xu, Z.; Zenobi, R. High-Spatial Resolution Atmospheric Pressure Mass Spectrometry Imaging Using Fiber Probe Laser Ablation-Dielectric Barrier Discharge Ionization. *Anal. Chem.* **2021**, *93*, 14694-14700.
(29) Otsuka, Y.; Kamihoriuchi, B.; Takeuchi, A.; Iwata, F.; Tortorella, S.; Matsumoto, T. High-spatial-resolution multimodal imaging by tapping-mode scanning probe electrospray ionization with feedback control. *Anal. Chem.* **2021**, *93*, 2263-2272.
(30) Nguyen, S. N.; Liyu, A. V.; Chu, R. K.; Anderton, C. R.; Laskin, J. Constant-distance mode nanospray desorption electrospray ionization mass spectrometry imaging of biological samples with complex topography. *Anal. Chem.* **2017**, *89*, 1131-1137.
(31) Nguyen, S. N.; Sontag, R. L.; Carson, J. P.; Corley, R. A.; Ansong, C.; Laskin, J. Towards high-resolution tissue imaging using nanospray desorption electrospray ionization mass spectrometry coupled to shear force microscopy. *J. Am. Soc. Mass. Spectrom.* **2017**, *29*, 316-322.
(32) Lanekoff, I.; Thomas, M.; Carson, J. P.; Smith, J. N.; Timchalk, C.; Laskin, J. Imaging Nicotine in Rat Brain Tissue by Use of Nanospray Desorption Electrospray Ionization Mass Spectrometry. *Anal. Chem.* **2013**, *85*, 882-889. DOI: 10.1021/ac302308p.
(33) Lanekoff, I.; Thomas, M.; Laskin, J. Shotgun Approach for Quantitative Imaging of Phospholipids Using Nanospray Desorption Electrospray Ionization Mass Spectrometry. *Anal. Chem.* **2014**, *86*, 1872-1880. DOI: 10.1021/ac403931r (acccessed 2014/02/07).
(34) Lanekoff, I.; Laskin, J. Imaging of lipids and metabolites using nanospray desorption electrospray ionization mass spectrometry. *Methods in molecular biology (Clifton, N.J.)* **2015**, *1203*, 99-106. DOI: 10.1007/978-1-4939-1357-2_10.
(35) Bergman, H.-M.; Lundin, E.; Andersson, M.; Lanekoff, I. Quantitative mass spectrometry imaging of small-molecule neurotransmitters in rat brain tissue sections using nanospray desorption electrospray

ionization. *Analyst* **2016**, *141*, 3686-3695, Article. DOI: 10.1039/c5an02620b.
(36) Duncan, K. D.; Fang, R.; Yuan, J.; Chu, R. K.; Dey, S. K.; Burnum-Johnson, K. E.; Lanekoff, I. Quantitative Mass Spectrometry Imaging of Prostaglandins as Silver Ion Adducts with Nanospray Desorption Electrospray Ionization. *Anal. Chem.* **2018**, *90*, 7246-7252, Article. DOI: 10.1021/acs.analchem.8b00350.
(37) Mavroudakis, L.; Stevens, S. L.; Duncan, K. D.; Stenzel-Poore, M. P.; Laskin, J.; Lanekoff, I. CpG preconditioning reduces accumulation of lysophosphatidylcholine in ischemic brain tissue after middle cerebral artery occlusion. *Anal Bioanal Chem* **2021**, *413*, 2735-2745. DOI: 10.1007/s00216-020-02987-w.
(38) Mesa Sanchez, D.; Brown, H. M.; Yin, R.; Chen, B.; Vavrek, M.; Cancilla, M. T.; Zhong, W.; Shyong, B.; Zhang, N. R.; Li, F.; et al. Mass spectrometry imaging of diclofenac and its metabolites in tissues using nanospray desorption electrospray ionization. *Anal. Chim. Acta* **2022**, *1233*, 340490-340490. DOI: 10.1016/j.aca.2022.340490.
(39) Mavroudakis, L.; Duncan, K. D.; Lanekoff, I. Host-Guest Chemistry for Simultaneous Imaging of Endogenous Alkali Metals and Metabolites with Mass Spectrometry. *Anal. Chem.* **2022**, *94*, 2391-2398, Article. DOI: 10.1021/acs.analchem.1c03913.
(40) Yang, M.; Hu, H.; Su, P.; Thomas, P. M.; Camarillo, J. M.; Greer, J. B.; Early, B. P.; Fellers, R. T.; Kelleher, N. L.; Laskin, J. Proteoform-Selective Imaging of Tissues Using Mass Spectrometry. *Angew. Chem. Int. Ed.* **2022**, e202200721.
(41) Su, P.; McGee, J. P.; Durbin, K. R.; Hollas, M. A.; Yang, M.; Neumann, E. K.; Allen, J. L.; Drown, B. S.; Butun, F. A.; Greer, J. B. Highly multiplexed, label-free proteoform imaging of tissues by individual ion mass spectrometry. *Science advances* **2022**, *8*, eabp9929.
(42) Hale, O. J.; Cooper, H. J. Native mass spectrometry imaging of proteins and protein complexes by nano-DESI. *Anal. Chem.* **2021**, *93*, 4619-4627.
(43) Hale, O. J.; Hughes, J. W.; Sisley, E. K.; Cooper, H. J. Native Ambient Mass Spectrometry Enables Analysis of Intact Endogenous Protein Assemblies up to 145 kDa Directly from Tissue. *Anal. Chem.* **2022**, *94*, 5608-5614. DOI: 10.1021/acs.analchem.1c05353.
(44) Yang, M.; Unsihuay, D.; Hu, H.; Nguele Meke, F.; Qu, Z.; Zhang, Z.-Y.; Laskin, J. Nano-DESI Mass Spectrometry Imaging of Proteoforms in Biological Tissues with High Spatial Resolution. *Anal. Chem.* **2023**, *95*, 5214-5222. DOI: 10.1021/acs.analchem.2c04795.
(45) Li, X.; Yin, R.; Hu, H.; Li, Y.; Sun, X.; Dey, S. K.; Laskin, J. An integrated microfluidic probe for mass spectrometry imaging of biological samples. *Angew. Chem.* **2020**, *132*, 22574-22577.
(46) Li, X.; Hu, H.; Yin, R.; Li, Y.; Sun, X.; Dey, S. K.; Laskin, J. High-throughput Nano-DESI Mass Spectrometry Imaging of Biological Tissues Using an Integrated Microfluidic Probe. **2022**.
(47) Helminiak, D.; Hu, H.; Laskin, J.; Hye Ye, D. Deep learning approach for dynamic sparse sampling for high-throughput mass spectrometry imaging. *Electronic Imaging* **2021**, *2021*, 290-291-290-297.
(48) Hu, H.; Helminiak, D.; Yang, M.; Unsihuay, D.; Hilger, R. T.; Ye, D. H.; Laskin, J. High-Throughput Mass Spectrometry Imaging with Dynamic Sparse Sampling. *ACS Measurement Science Au* **2022**.
(49) Iliescu, C.; Taylor, H.; Avram, M.; Miao, J.; Franssila, S. A practical guide for the fabrication of microfluidic devices using glass and silicon. *Biomicrofluidics* **2012**, *6*, 016505.
(50) Lanekoff, I.; Heath, B. S.; Liyu, A.; Thomas, M.; Carson, J. P.; Laskin, J. Automated platform for high-resolution tissue imaging using nanospray desorption electrospray ionization mass spectrometry. *Anal. Chem.* **2012**, *84*, 8351-8356.
(51) Colliver, T. L.; Brummel, C. L.; Pacholski, M. L.; Swanek, F. D.; Ewing, A. G.; Winograd, N. Atomic and molecular imaging at the single-cell level with TOF-SIMS. *Anal. Chem.* **1997**, *69*, 2225-2231.
(52) Luxembourg, S. L.; Mize, T. H.; McDonnell, L. A.; Heeren, R. M. High-spatial resolution mass spectrometric imaging of peptide and protein distributions on a surface. *Anal. Chem.* **2004**, *76*, 5339-5344.
(53) Heiles, S.; Kompauer, M.; Müller, M. A.; Spengler, B. Atmospheric-Pressure MALDI Mass Spectrometry Imaging at 213 nm Laser Wavelength. *J. Am. Soc. Mass. Spectrom.* **2020**, *31*, 326-335. DOI: 10.1021/jasms.9b00052.
(54) Spraggins, J. M.; Caprioli, R. M. High-Speed MALDI-TOF Imaging Mass Spectrometry: Rapid Ion Image Acquisition and Considerations for Next Generation Instrumentation. *J. Am. Soc. Mass. Spectrom.* **2011**, *22*, 1022-1031. DOI: 10.1007/s13361-011-0121-0.
(55) Ma, T.; Mao, W.; Zhang, S.; Wang, Y.; Wang, T.; Liu, J.; Shi, L.; Yu, X.; Xue, R.; Shui, G.; et al. Ablation of Mea6/cTAGE5 in oligodendrocytes significantly impairs white matter structure and lipid content. *Life Metabolism* **2023**. DOI: 10.1093/lifemeta/load010 (acccessed 4/24/2023).
(56) Poitelon, Y.; Kopec, A. M.; Belin, S. Myelin Fat Facts: An Overview of Lipids and Fatty Acid Metabolism. *Cells* **2020**, *9*, 812.

Table of Contents